Journal of Physics: Conference Series **568** (2014) 052030 doi:10.1088/1742-6596/568/5/052030

Observation and calculation of higher-order sideband transitions in a flux qubit coupled to a SQUID-based resonator

Y Shimazu[1], **R Shirasaki, S Toda and H Yamanashi**

Yokohama National University, 79-5 Tokiwadai, Hodogaya, Yokohama 240-8501, Japan

[1]E-mail: yshimazu@ynu.ac.jp

Abstract. Qubit–resonator coupled systems have been intensively studied because of their potential usefulness in quantum information processing. We investigated a superconducting flux qubit coupled to a resonator mode (SQUID plasma mode) associated with a dc SQUID used to read out the qubit state. Higher-order red and blue sideband transitions with $|M| = 1$, 2, and 3, where M represents the change in the quantum number of the resonator state, were clearly observed away from the symmetry point. We calculated the transition matrix elements between the dressed states and examined their dependence on both the coupling strength and the flux bias for the qubit. The observation of the sidebands up to $|M| = 3$ is consistent with the calculation results.

1. Introduction

Circuit quantum electrodynamics (QED) systems [1], in which superconducting qubits are coupled to a resonator, are considered to be important hybrid quantum systems for applications in quantum information processing. Recently, we have shown experimental results of higher-order sideband transitions with $|M| = 1$ and 2 and sideband Rabi oscillations on a flux qubit coupled to a SQUID-based resonator deep in the dispersive regime [2], where M represents the change in the quantum number of the resonator state. Higher-order sideband transitions in a superconducting qubit coupled to a resonator have also been reported with the use of a linear LC resonator [3] and a micromechanical resonator [4]. In quantum information processing, these sideband transitions may be useful for building quantum gates [5].

In this paper, we present experimental results from a flux qubit coupled to a SQUID-based resonator with enhanced coupling strength compared with that of our previous study. We observed higher-order sideband transitions with $|M|$ up to 3. To elucidate the origin of these transitions, we calculated the relevant transition matrix elements. The calculated results are consistent with our experimental results.

2. Experimental

Figure 1 shows a schematic of the sample, which was fabricated using electron-beam lithography and angled aluminum deposition. The three-Josephson-junction flux qubit [6] is galvanically connected to the readout dc SQUID. The effective area of the Al shunt capacitor is ~2000 μm^2. The qubit is

[1] To whom any correspondence should be addressed.

dominantly coupled to a single arm of the dc SQUID [7], in contrast to the conventionally studied flux qubits with symmetric geometry [8–10]. In our geometry, the qubit–SQUID coupling is considerably larger at zero bias current at the expense of higher susceptibility to bias-current noise. This large coupling enabled us to observe higher-order sideband transitions [2]. The measurement was performed at 20 mK. For spectroscopy and measurement of Rabi oscillations, the switching probability P_{sw} of the SQUID was recorded using a short bias-current pulse applied to the SQUID immediately after a microwave pulse [8].

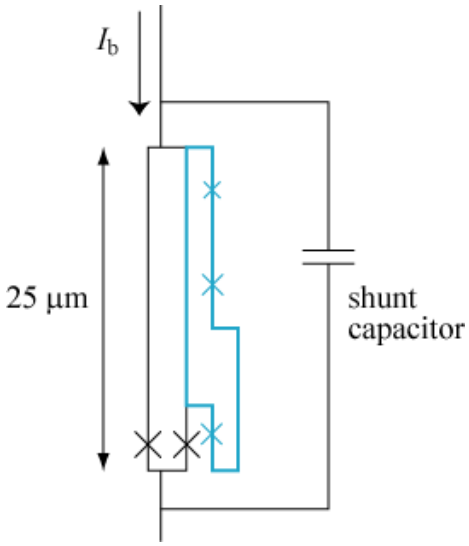

Figure 1. (color online) Schematic diagram of the sample. The crosses represent small Josephson junctions (JJ). The blue loop with three JJ represents a three-JJ flux qubit, which is coupled to the single arm of the dc SQUID. The frequency of the SQUID plasma mode can be tuned via the bias current I_b and the magnetic flux in the SQUID loop.

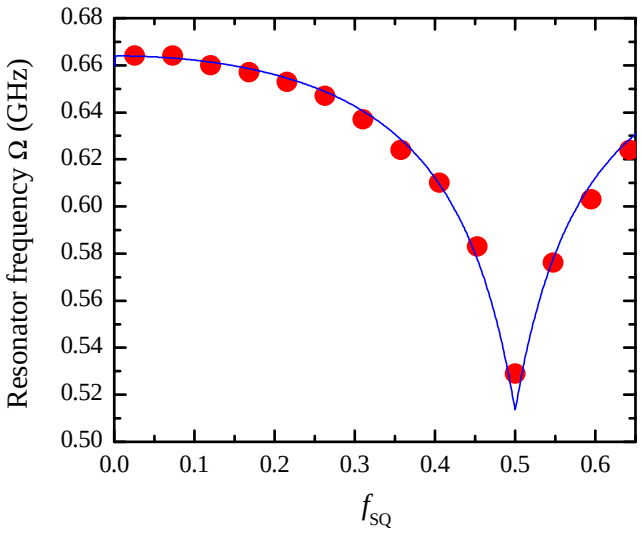

Figure 2. (color online) The resonator frequency, that is, the frequency of the SQUID plasma mode, as a function of $f_{SQ} = \Phi_{SQ}/\Phi_0$, where Φ_{SQ} is the magnetic flux threading the SQUID loop. The parameters used for the calculated result shown by the line are as follows: minimum Josephson inductance of the dc SQUID L_{SQ} = 280 pH, stray inductance L_s = 1560 pH, shunt capacitance C = 31 pF, and normalized SQUID-loop inductance $\beta = 2LI_c/\Phi_0 = 0.12$, where L and I_c are the SQUID-loop inductance and the critical current of each SQUID junction, respectively.

3. Results and discussion

As shown later, sideband transitions were observed at frequencies separated by ~0.6 GHz. The resonator mode of ~0.6 GHz was indeed observed as a sharp resonant peak in P_{sw}, which was apparent at temperatures as high as 0.5 K. The dependence of the resonant frequency on $f_{SQ} = \Phi_{SQ}/\Phi_0$, where Φ_{SQ} is the magnetic flux threading the SQUID loop and $\Phi_0 = h/2e$, is shown in figure 2. This resonance is attributed to the SQUID plasma mode [9,10] that is an LC resonance involving the Josephson inductance of the SQUID, the stray inductance, and the shunt capacitance C. The observed resonant frequency Ω is in good agreement with the calculated frequency of the SQUID plasma mode as shown in figure 2. In the calculation, a loop inductance for the SQUID of reasonable magnitude was required to attain good agreement with the experimental data.

In the spectroscopic measurement of the qubit, we observed higher-order red- and blue-sideband transitions, as shown in figure 3, under strong microwave drive and away from the symmetry point. The peak frequency is given by $\nu_Q + M\Omega$, where ν_Q = 9.9 GHz is the qubit transition frequency. These sidebands are attributed to the transitions among energy levels of the dressed states of the qubit–resonator coupled system. The resonator energy $\Omega \sim 0.6$ GHz corresponding to 30 mK should be below the thermal energy; the effective temperature of the system is estimated to be ~200 mK on the basis of the width of the qubit step [11]. Therefore, a significant amount of photons is thermally excited, in contrast to the case of the previous study with $\Omega \sim 3$ GHz [9]. These thermally excited photons seed the red-sideband generation process. In figure 3, the transitions with $|M| = 1$, 2, and 3 are clearly shown. This result is compared with that of our previous measurement on a similar sample [2], where only the transitions with $|M| \leqq 2$ were clearly observed. We ascribe this difference to the enhanced coupling strength between the qubit and the resonator. The critical current of the SQUID in the present sample is higher by a factor of approximately four compared with the previous sample, which should lead to enhanced coupling strength.

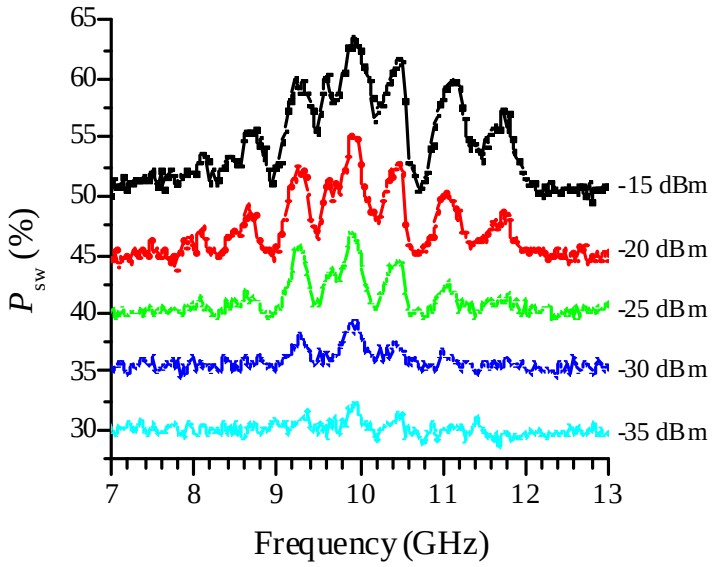

Figure 3. (color online) P_{sw} as a function of microwave frequency for various values of microwave power, measured at I_b = 0 and cos θ = 0.84. The duration of the microwave pulse was 100 ns. The traces are offset vertically for clarity. With increasing power, sideband transitions of higher orders appear beside the carrier transition.

We calculated the matrix elements that are relevant to the observed sideband transitions. The energy eigenvectors of the qubit–resonator system can be derived by diagonalizing the coupled Hamiltonian [2,12],

$$H_{QR} = \frac{h}{2}\nu_Q\sigma_z + h\Omega(a^\dagger a + \frac{1}{2}) + hg(\sigma_z \cos\theta - \sigma_x \sin\theta)(a^\dagger + a),$$

where g is the qubit–resonator coupling constant, $\cos\theta = \sqrt{1-(\Delta/\nu_Q)^2}$, and Δ is the qubit energy gap [6]. Deep in the dispersive regime, which is the case for the sample under investigation, the eigenvectors can be labeled as $|g\ n\rangle$ and $|e\ n\rangle$ using the labels of the dominant bare states; the bare states are the eigenstates of $\frac{h}{2}\nu_Q\sigma_z + h\Omega(a^\dagger a + \frac{1}{2})$. Here, g and e denote the ground and excited states of the qubit, respectively, and n is the photon number. The transition matrix elements for the sideband transition from the initial state $|g\ n\rangle$ changing the photon number by M is given by

$$T(n, M) = |\langle e\ n+M\ |(\sigma_z \cos\theta - \sigma_x \sin\theta)|\ g\ n\rangle|.$$

In order to compare these calculated results with the data shown in figure 3, $T(n, M)$ was calculated by fixing the parameters as ν_Q = 9.9 GHz, Ω = 0.6 GHz, and cos θ = 0.84. Since the coupling constant g is unknown from the experimental data obtained thus far, g was varied from 0.05 to 0.2 GHz. We believe that these values are in the relevant range, in view of g = 0.1 GHz estimated for a separate

sample [2]. In a future experiment, g will be estimated for the present sample by using a spectroscopic measurement in which the bias current is varied. Because several photons are thermally excited, $T(n, M)$ for n ranging from 0 to 5 is shown here. With increasing g, $T(n, M)$ with higher M increases, as expected. For g higher than 0.15 GHz, $T(n, M)$ with $|M| = 3$ has appreciable magnitude, which is consistent with our observation of transitions with $|M| = 3$. Interestingly, for the higher values of g and n, $T(n, M)$ with nonzero M is larger than $T(n, 0)$. The appearance of the higher-order sideband transitions reflects the fact that the eigenstate consists of several photon-number states. If we assume that the coupled Hamiltonian is of Jaynes-Cummings type [1], the eigenstate consists of two bare states and only transitions with M = 0, -1, and -2 are possible. Experimentally, we observed that the sideband transitions are gradually suppressed as the operating point approaches the symmetry point ($\theta = \pi/2$). This behavior was also described in the calculation of $T(n, M)$.

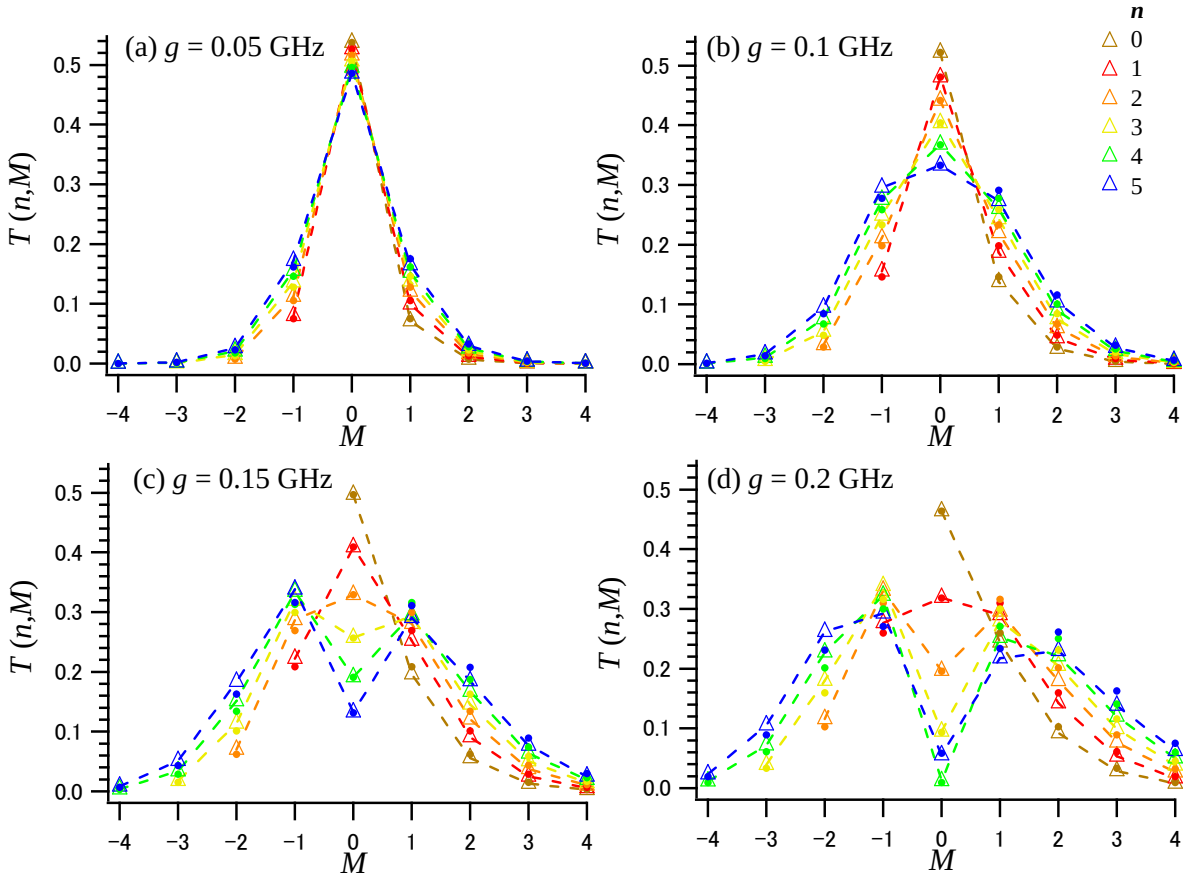

Figure 4. (color online) Transition matrix elements for the transition in which the photon number is changed by M; $T(n, M) = |\langle e, n+M|(\sigma_z \cos\theta - \sigma_x \sin\theta)|g, n\rangle|$ for g = 0.05, 0.1, 0.15, and 0.2 GHz. The parameters used for the calculation are ν_Q = 9.9 GHz, Ω = 0.6 GHz, and $\cos\theta$ = 0.84. The values denoted with triangles are obtained using the eigenstates of H_{QR}, while the values denoted with dots are obtained using those of H_{QR}'.

If we neglect the term $-hg\,\sigma_x \sin\theta(a^+ + a)$ in H_{QR}, the eigenstates of the resulting Hamiltonian

$$H_{QR}' = \frac{h}{2}\nu_Q\sigma_z + h\Omega(a^\dagger a + \frac{1}{2}) + hg\sigma_z \cos\theta(a^\dagger + a)$$

can be analytically derived using a displacement operator for the harmonic oscillator states [13]. We found that the transition matrix elements between the eigenstates of H_{QR}' nearly agree with those

between the eigenstates of H_{QR} for the parameters used in the calculation, as indicated by the dots and triangles, respectively, in figure 4.

To understand this agreement, we consider the eigenstates of H_{QR} and H_{QR}'. In general, the eigenstates of H_{QR} can be written as

$$|g\ n\rangle = \sum_k G_k^{g,n} |g\ k\rangle^{(0)} + \sum_k E_k^{g,n} |e\ k\rangle^{(0)} \text{ and } |e\ n\rangle = \sum_k G_k^{e,n} |g\ k\rangle^{(0)} + \sum_k E_k^{e,n} |e\ k\rangle^{(0)},$$

where $|g\ k\rangle^{(0)}$ and $|e\ k\rangle^{(0)}$ are the bare states of the system. Meanwhile, the eigenstates of H_{QR}' can be written as

$$|g\ n\rangle' = \sum_k \tilde{G}_k^{g,n} |g\ k\rangle^{(0)} \text{ and } |e\ n\rangle' = \sum_k \tilde{E}_k^{e,n} |e\ k\rangle^{(0)},$$

because H_{QR}' does not couple the qubit ground state |g > with the qubit excited state |e >. Deep in the dispersive regime, which is the case considered in this study, we observe that the $E_k^{g,n}$ terms in $|g\ n\rangle$ and the $G_k^{e,n}$ terms in $|e\ n\rangle$ are very small. This is because these terms are proportional to $g \sin\theta/\nu_Q$, as derived from the first-order perturbation theory. Subsequently, we note that the matrix elements of H_{QR} and H_{QR}' in the subspace spanned by $|g\ k\rangle^{(0)}$ (or $|e\ k\rangle^{(0)}$) are the same:
$^{(0)}\langle g\ k | H_{QR} | g\ k'\rangle^{(0)} = {}^{(0)}\langle g\ k | H_{QR}' | g\ k'\rangle^{(0)}$ and $^{(0)}\langle e\ k | H_{QR} | e\ k'\rangle^{(0)} = {}^{(0)}\langle e\ k | H_{QR}' | e\ k'\rangle^{(0)}$. Given the aforementioned considerations, we conclude that the eigenstates of H_{QR} are approximately equal to those of H_{QR}'. Therefore, the transition matrix elements between the eigenstates of H_{QR}' nearly agree with those between the eigenstates of H_{QR}. The substitution of H_{QR}' for H_{QR} may be advantageous in some analyses because the eigenstates of H_{QR}' can be analytically derived.

The transition matrix element is closely related to the period of Rabi oscillations associated with the transition. We have shown that the coupling constant can be estimated from the ratio between the Rabi periods for the carrier transition and the sideband transitions [2]. For the sample under investigation, although we have observed Rabi oscillations for the sideband transition, quantitative analysis of the Rabi periods on the basis of the calculated $T(n, M)$ has not been performed, partly because of the unknown coupling constant and the significant frequency dependence of the microwave attenuation, which strongly affects the ratio between the Rabi periods for different transitions. Further measurement and analysis will be performed in a future experiment. In the sample studied here with a relatively small value of Ω, the significant amount of thermal excitation of photons causes difficulty in analyzing the data and photon noise [10], leading to a short coherence time. However, this system may become a feasible platform for quantum operations involving many dressed states with easily accessible energies, including sideband cooling of the resonator.

4. Conclusion

In conclusion, we observed higher-order red- and blue-sideband transitions with $|M| = 1$, 2, and 3 in a coupled system of a flux qubit and a SQUID-based resonator, the coupling strength of which is larger than that of a similar sample we studied previously. Higher-order red sidebands were observed in a simple scheme because the resonator was strongly excited by thermal energy. The significant qubit–resonator coupling at $I_b = 0$ in these observations was due to the sample geometry; the qubit was coupled to a single arm of the dc SQUID. We calculated transition matrix elements between the dressed states obtained by diagonalizing the coupled Hamiltonian. The appearance of the sidebands up to $|M| = 3$ is consistent with the results of calculations in which reasonable coupling strength is assumed. The observed suppression of the sideband transition near the symmetry point is also consistent with the calculated transition matrix elements.

Acknowledgments

This work was supported by JSPS KAKENHI Grant Number 24540317.

References

[1] Blais A, Huang R S, Wallraff A, Girvin S M and Schoelkopf R J 2004 *Phys. Rev.* A **69** 062320
[2] Shimazu Y, Takahashi M and Okamura N 2013 *J. Phys. Soc. Jpn.* **82** 074710
[3] Plantenberg J H 2007 Ph. D. Thesis (Delft University of Technology)
[4] Pirkkalainen J M, Cho S U, Li J, Paraoanu G S, Hakonen P J and Sillanpaa M A 2013 *Nature* **494** 211
[5] Blais A, Gambetta J, Wallraff A, Schuster D I, Girvin S M, Devoret M H and Schoelkopf R J 2007 *Phys. Rev.* A **75** 032329
[6] Mooij J E, Orlando T P, Levitov L S, Tian L, van der Wal C H and Lloyd S 1999 *Science* **285** 1036, Orlando T P, Mooij J E, Tian L, van der Wal C H, Levitov L S, Lloyd S, and Mazo J J 1999 *Phys. Rev.* B **60** 15398
[7] Shimazu Y, Nakajima M, Takahashi M, Okamura N and Yoshiyama K 2012 *Physics Procedia* **27** 360
[8] Chiorescu I, Nakamura Y, Harmans C J P M and Mooij J E 2003 *Science* **299** 1869
[9] Chiorescu I, Bertet P, Semba K, Nakamura Y, Harmans C J P M and Mooij J E 2004 *Nature* **431** 159
[10] Bertet P, Chiorescu I, Burkard G, Semba K, Harmans C J P M, DiVincenzo D P and Mooij 2005 *Phys. Rev. Lett.* **95** 257002
[11] van der Wal C H, ter Haar A C J, Wilhelm F K, Schouten R N, Harmans C J P M, Orlando T P, Lloyd S and Mooij J E 2000 Science **290** 773
[12] Fedorov A, Feofanov A K, Macha P, Forn-Díaz P, Harmans C J P M and Mooij J E 2010 *Phys. Rev. Lett.* **105** 060503
[13] Scully M O and Zubairy M S 1997 *Quantum Optics* (Cambridge University Press)